Research Article

Baskar Thangaraj* and Krishnan Mahadevan

Corrosion studies of DC reactive magnetron sputtered alumina coating on 304 SS

https://doi.org/10.1515/eetech-2017-0001
Received Jun 04, 2017; accepted Sep 14, 2017

Abstract: Aluminum oxide films on SS 304 deposited by DC reactive magnetron sputtering technique were studied with respect to the composition of the sputter gas ($Ar:O_2$), gas pressure, substrate temperature, current etc. to achieve good insulating films with high corrosion resistance. The films were characterized by XRD and SEM techniques. Potentiodynamic polarization and electrochemical impedance spectroscopy measurements were made under static conditions in order to evaluate the corrosion performance of the alumina-coated SS 304 for various immersion durations in 0.5 M and 1 M NaCl solution. Alumina-coated SS 304 has low corrosion value of 0.4550 and 1.1090 MPY for 24 h immersion time in both solutions. The impedance plots for the alumina coated SS 304 in 1 M NaCl solution at different durations are slightly different to when compared to its immersion in 0.5 M NaCl solutions and are composed of two depressed semi circles. For the alumina coated film, the impedance spectrum decreased, when immersion time increased.

Keywords: aluminum oxide; DC reactive sputtering; electrochemical corrosion

1 Introduction

Amorphous alumina (aluminum oxide) thin films have many applications and have attracted much attention during the past 20 years [1]. Aluminum oxide thin films are widely used in many mechanical, optical and microelectronic applications [2]. Due to the mechanical, electrical, thermal and optical properties of aluminum oxide, it has become an important thin film material for various applications [3] (*e.g.*, protective coatings, diffusion barriers, electronic seals, dielectric layers and optical layers etc.,) [4]. Aluminum oxide has high melting temperature, hardness, abrasion and oxidation resistance, and finds application in cutting tools in conjunction with other hard coating materials like TiN, TiCN and TiC [5], it also provides the corrosion resistance of aluminum [6]. The aluminum oxide thin film can reduce the oxidation rate of superalloys [4]. Due to its high electrical resistivity, alumina coatings are also of interest in the microelectronics industry [5]. This is due to its high electrical breakdown field, its large band gap and its high dielectric constant [7]. The large band gap of aluminum oxide, for example, facilitates its use in a magnetic tunnel junction, the low thermal conducting, on the other hand makes it a very suitable material for thermal barrier coatings as they are used e.g. in gas turbine engines [3]. Complexities in the properties of alumina exist due to the presence of a wide range of different crystalline phases such as α, γ, δ, η, χ, θ and k-alumina [8, 9]. α–Al_2O_3can be deposited by chemical vapor deposition (CVD) and physical vapor deposition (PVD) [10]. Generally, the crystalline structure of α, k and θ-Al_2O_3 is formed by chemical vapor deposition, while η and γ phases are formed by oxidation of aluminum metal, depending on the conditions. Depending on the technique selected and its processing parameters, various options are available for surface modifications [10].

Chemical vapor deposition is widely used to deposit alumina coatings (usually k-alumina) at 700 - 1000°C [11]. This process generally ensures good bonding between the substrate and the grown film, but the thermal expansion mismatch leads to the buildup of residual stress upon cooling that adversely affects adhesion though crack generation. These CVD methods also prohibit the coating of high-speed steel (HSS) [12]. Thus the choice of substrate is limited because of high deposition temperature as required for the formation of the stable α-Al_2O_3. This drawback can be minimized by using physical vapor deposition (PVD) operating at lower temperatures. Additionally, PVD techniques offer the advantage of introducing compressive stresses in the coatings which lead to enhanced fatigue and thermal shock resistance [8]. PVD techniques such as e-beam evaporation, pulsed laser deposition and reactive

***Corresponding Author: Baskar Thangaraj:** Department of Physics (PG), Sourashtra College, Madurai -625004, Tamil Nadu, India; Email: biodieselbaskar@yahoo.co.in
Krishnan Mahadevan: Department of Physics (PG), Sourashtra College, Madurai -625004, Tamil Nadu, India

Table 1: Chemical composition of 304 SS

Grade		C	Mn	Si	P	S	Cr	Mb	Ni	N	Fe
	Min	-	-	-	-	-	18.0	-	8.0	-	Balance
304	max	0.08	2.0	0.75	0.045	0.03	20.0	-	10.5	0.10	Balance

sputtering have been used to deposit amorphous Al_2O_3 at low temperatures. To obtain α phase, the amorphous film is subjected to a temperature of 750°C or more during post-synthesis annealing [12]. The first breakthrough for PVD α-Al_2O_3 was made in 1996 by Zywitzki *et al*. in which crystalline α-alumina was deposited on steel substrate at temperatures ranging from 750 - 770°C by using the pulsed reacting dual magnetron sputtering process [13]. This work was followed by Yamada *et al*. who reported on the reactive deposition of α-Al_2O_3 from a filtered vacuum arc at 780°C [14]. The lowest temperature for the deposition of α-alumina in the literature is 280°C [15] and the maximum deposition rate reported was 150 nm/h [11]. The process of reactive sputter deposition involves (1) the sputtering process (2) the physics of the plasma discharge (3) transport of the sputtered and gas species (4) the kinetics of film growth (5) and the chemical interactions at the target and film surfaces. One of the main advantages of DC magnetron sputtering is the high deposition rate, especially of metals in an inert gas atmosphere. Reactive sputtering is currently preferred for depositing dielectrics such as oxides and nitrides, as well as carbides and silicides, among which aluminum oxide is of particular interest because of its wide applications in material coating technologies for the protection of metallic components operating in hostile corrosive or oxidative environments [16]. The work presented here reports a systematic study of DC reactive magnetron sputtering Al_2O_3 coatings applied to stainless steel 304. The corrosion properties of the coated substrates in aqueous solutions of 0.5 and 1 M NaCl were studied by potentiodynamic polarization and electrochemical impedance (EIS) measurements. The Al_2O_3 films before and after corrosion studies were characterized by XRD and SEM techniques.

2 Experimental

The chemical composition of 304 SS is given in Table 1. The deposition technique used was DC reactive sputtering (Hind High Vacuum Co (p) Ltd, Bangalore.) from an aluminum target. The purity of aluminum was 99.99 wt%. The effective sputtering area on the circular target was about 19.64 cm^2 and its thickness was about 0.35 cm. The average distance between the substrate and target was about 7 cm. High purity (99.997%) argon gas was fed into the chamber as the working gas for forming plasma vaporized with a constant flow rate of 10 sccm. High purity oxygen was sent to the chamber through a mass flow controller and was allowed to react with the sputtered metal species to produce desired oxide coating. The substrate was used a stainless steel 304. The substrate area was 1 ×1 cm^2 and 1× 2.5 cm^2 respectively. The substrate was scrubbed by using different grade emery papers 600, 800, 1000 and 1200, it was then cleaned chemically with 2-propanol and acetone for 15 min in an ultrasonic bath. The vacuum chamber was evacuated by a vacuum pump yielding a bare pressure of 7 ×10^{-6} mbar. Ar and O_2 gas flow rates were controlled by independent mass flow controllers. The Ar and O_2 gas flow rates were 10 sccm and 3 sccm respectively. Argon was introduced into the target housing and oxygen was introduced immediately in front of the substrate holder. The sputter pressure range was 1 ×10^{-3} mbar. During sputtering in pure Ar, the color of the sputter target changed from blue to bluish pink due to the enrichment of Al by preferential sputtering of oxygen. The temperature was not controlled at the substrate; the sputtering process was carried out at room temperature and a constant current rate of nearly 0.12 A. Before the deposition process, the target was pre-cleaned well for removing the impurities on the target surface, which is known as an etching process. The etching process was carried out for 15 min. After the etching process, the deposition was carried out for a longer time like 45 min for making a thin film.

3 Results and discussion

Aluminum oxide film was prepared by DC reactive magnetron sputtering. The oxygen flow rate was chosen 3 sccm for preparing aluminum oxide film. The growth rate of aluminum oxide thin films increases with the oxygen flow rate from 1 sccm to 3 sccm. The crystallinity of aluminum oxide thin films increases with the oxygen flow rate from 1 to 3 sccm and decreases above 3 sccm. The maximum of crystallinity indicates the competition of different effects

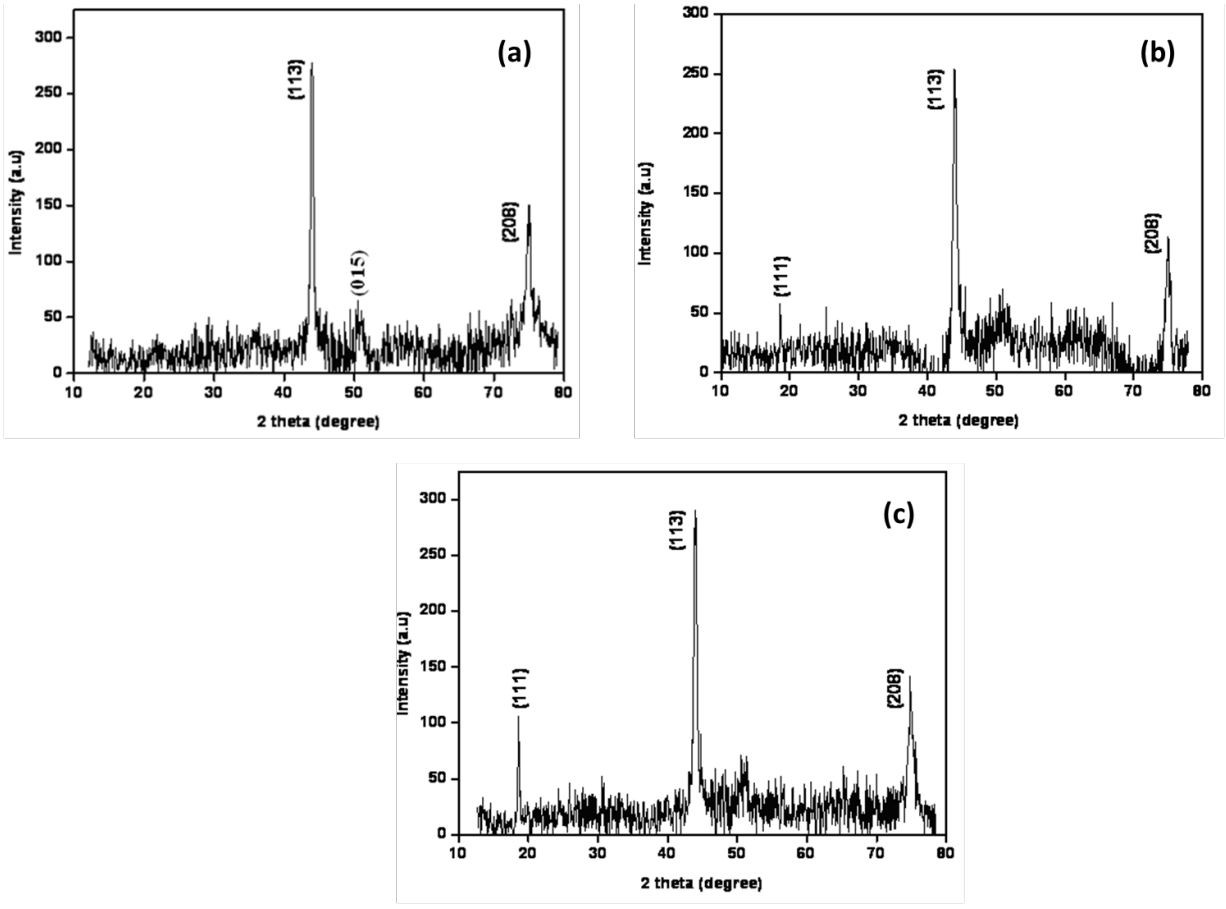

Figure 1: X-ray diffraction pattern of alumina coated SS 304 (a) before immersion in NaCl and (b) after immersion period of 24 h in 0.5 M NaCl (c) after immersion period of 24 h in 1 M NaCl.

of oxygen flow. One of these effects is the formation of inclusions. The aluminum oxide thin film prepared at 3 sccm oxygen flow rate has fewer inclusions caused by target poisoning at high oxygen flow rate and has less inclusion than that prepared at 1 sccm. These inclusions are caused by target poisoning at high oxygen flow and by the metal droplets from the aluminum target at low oxygen flow. Meanwhile, the oxygen content approaching that of pure alumina improves the formation of alumina nanocrystals. However, the effects of target poisoning and plasma reduction with increasing oxygen flow rate over 3 sccm were dominating. The outcome of both effects is the porous structure of aluminum oxide thin films. Also caused by this effect is the vanishing of the crystallinity of the aluminum oxide thin films. This result shows that the lowering of the kinetic energy of depositing ions in the plasma inhibits the formation of more neutral particles [9]. For these reasons, an oxygen flow rate of 3 sccm and argon flow rate of 10 sccm are maintained. The sputtering current was maintained at 0.12A and the corresponding voltage was around 270 V. Changes in current during deposition were compensated by oxygen gas flow rate to maintain the target voltage in the nominal range of 270 V. The oxygen flow rate may slightly decrease to maintain constant target voltage during deposition due to the target poisoning. In the voltage-controlled deposition, the value of the target voltage of metallic aluminum has to be taken as reference value [17]. The sputtering current 0.12 A gives a sufficient plasma vaporization region for effective reactive gas sputtering.

XRD patterns of the alumina coated 304 SS films were recorded by using XPERT-PRO diffractometer system using Cu kα radiation (Kα1-1.54060Å, Kα2-1.54443 Å, K$\alpha\beta$-1.39225 Å). The measurements were recorded in steps of 0.5000° with a scan step time of 10.1382 and a 2θ range 2-80° at an operating voltage of 40 kV at 30 mA. The crystalline sizes were calculated by Scherrer's equation

$$C_s = \frac{0.94 \times \lambda}{\beta \cos\theta} \text{ nm}$$

where C_s stands for the size of the particle, λ is the X-ray wavelength, β is the full width at half maximum (FWHM), θ is the diffraction angle.

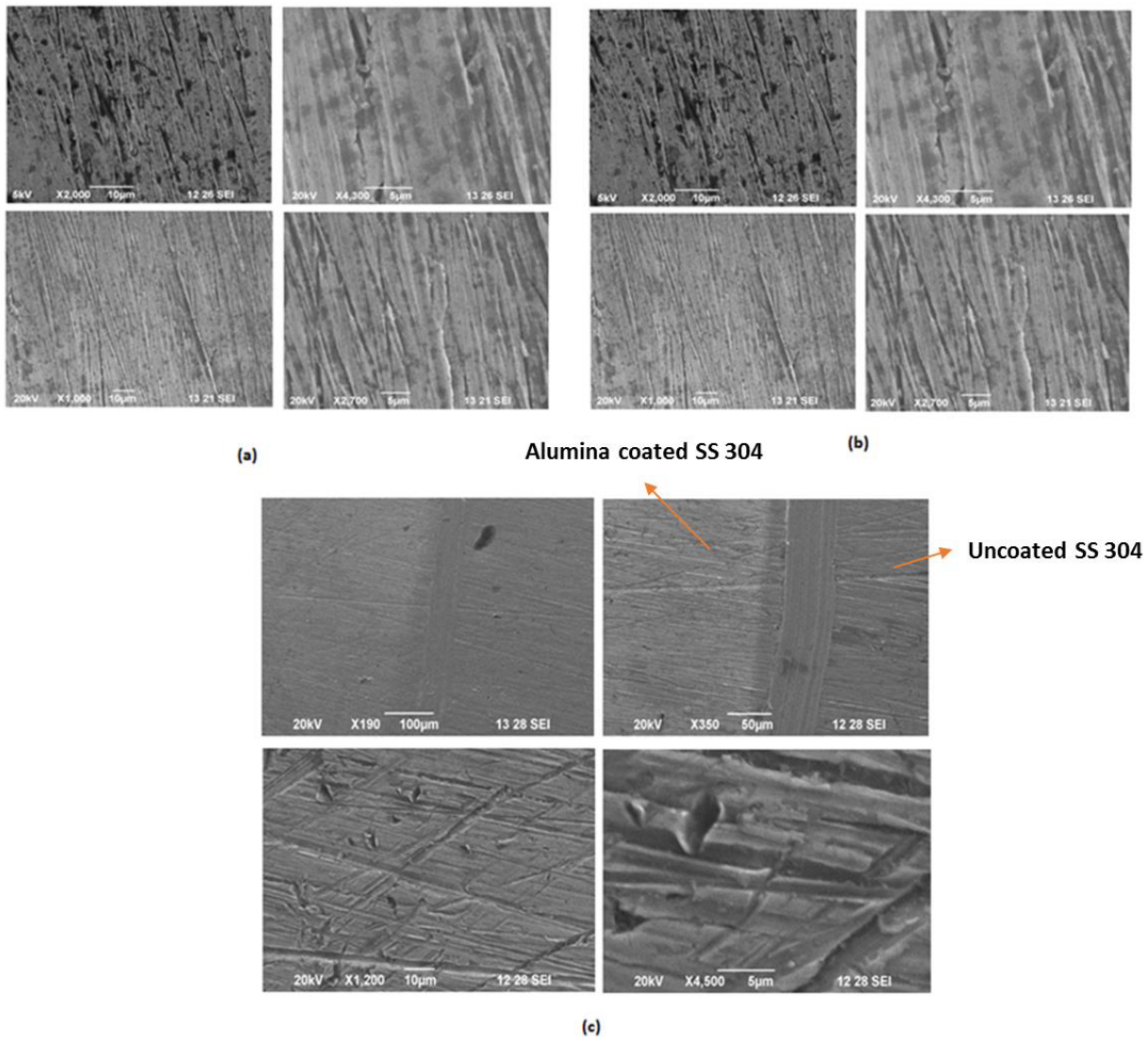

Figure 2: SEM images of alumina coated SS 304 (a) before immersion in NaCl and (b) after immersion period of 24 h in 0.5 M NaCl (c) after immersion period of 24 h in 1 M NaCl.

The X-ray diffraction pattern of the sputtered alumina on SS 304 before and after immersion for 24 h in 0.5 and 1 M NaCl is shown in Figure 1. The crystal structures and phases of the alumina were ascertained from the XRD-pattern. Bragg peaks at 2θ values at 43° and 74° are attributed to (113) and (208) planes in α-Al_2O_3, with particle sizes ranging from 10.5 to 13.5 nm. The α-Al_2O_3 is in a hexagonal structure [a = 4.758 Å, C = 12.99 Å] and Rhomb-centered lattice system with six formula units in each unit cell and it has space group $R\bar{3}C$ [JCPDS file card No: 05 - 0712].

The morphology of the alumina coated 304 SS film was measured by scanning electron microscopy (Model: JEOL-6390, and acceleration voltage 0.5-30 kV) at a magnification range of 5 to 300,000. The surface morphology is given in Figure 2 (a-c) at various resolutions. The surface defect that occurs during polishing is still visible in this film indicating very thin film deposition. The study reveals that better surface coverage of the films corresponds to deposition in the transition region.

PARSTAT 2273 potentiostat was used for the electrochemical measurements of potentiodynamic polarization in a conventional three-electrode cell. Pt foil was used as an auxiliary electrode, saturated calomel electrode SCE was the reference (all the potentials hereafter will be referred to SCE), and pure alumina coated stainless 304 SS plates (0.3 mm thickness, with a surface area equal to 1 × 1 cm^2) were used as working electrodes. Frequencies in impedance measurements were chosen in the range from 1 to 10 MHz with the amplitude of the sinusoidal voltage

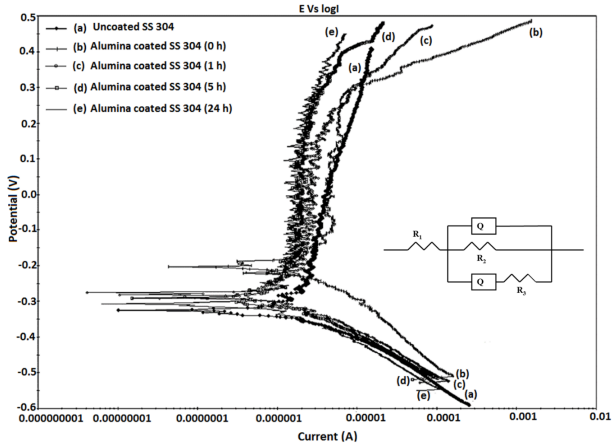

Figure 3: Potentiodynamic polarization curve for uncoated 304 SS and alumina coated 304 SS in 0.5 M NaCl solution at different immersion times (a) Uncoated SS 304, (b) alumina coated SS 304 in 0h, (c) Alumina coated SS 304 in 1 h, (d) alumina coated SS 304 in 5 h (e) alumina coated SS 304 in 24 h.

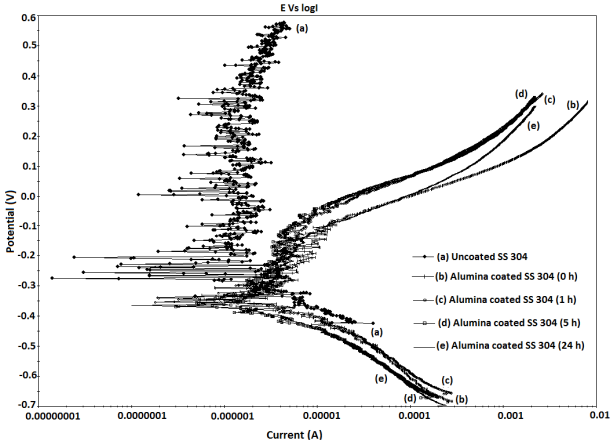

Figure 4: Potentiodynamic polarization curve for uncoated 304 SS and alumina coated 304 SS in 1 M NaCl solution at different immersion times (a) Uncoated SS 304, (b) alumina coated SS 304 in 0h, (c) Alumina coated SS 304 in 1 h, (d) alumina coated SS 304 in 5 h (e) alumina coated SS 304 in 24 h.

signal of 25 mV/s at the open circuit potential (0.10026 V). They were carried out after different immersion times varying from 1 to 24 h. All the recorded impedance spectra were displayed as Bode and Nyquist diagrams. Using the Zsim Win (3.21) software theoretical models (described by a simple equivalent circuit diagram) for the impedance spectra were selected. Potentiodynamic polarization results for the anodized samples and the original stainless steel 304 in a 0.5 M and 1 M NaCl solution are shown in Figure 3 and 4. There is a considerable decrease in the anodic current of the anodized samples compared to the uncoated 304 SS. The current density (I_{corr}/μA) of the anodized samples was significantly lower (about one order of magnitude) than that of the uncoated 304 SS. The corrosion protection efficiency of the alumina coatings is evident from both the increase in corrosion potential as well as the reduction in the corrosion current density.

Corrosion potentials (E_{corr}/mV), current densities and anodic/cathodic Tafel slopes (β_{an} & β_{ca}) were obtained from these results. Then based on the approximate linear polarization resistance at the corrosion potential polarization resistance (R_p) values were determined using the relationship

$$R_p = \frac{\beta_{ca} \times \beta_{an}}{2.3 I_{corr} (\beta_{ca} + \beta_{an})} \ \Omega/\text{cm}^2$$

Corrosion rate can be calculated by using the formula

$$CR = \frac{C \times EW \times I_{corr}}{d \times A} \ /\text{MPY}$$

Where

CR - Corrosion rate in milli inches per year (MPY)

C - Conversion constant (*i.e.* 1.287×10^5)

EW - Equivalent weight of the sample (304 SS) in gm (25.12 gm)

d - Density of the sample (304 SS) (7.9 gm/cm^3)

I_{corr} - Corrosion current density (μA)

A - Area of the sample (304 SS) (1 cm^2)

Inhibition efficiency (IE) can also be found using the following relationship

$$IE = \frac{(CR^\circ - CR)}{CR^\circ} \ (\%)$$

where, CR$^\circ$ and CR are the corrosion rates without and with alumina coating, respectively. A summary of the results of the potentiodynamic corrosion tests is given in Table 2 and 3.

All coated samples at different immersion times showed higher corrosion resistance than the 304 SS substrate (all are increased by about one order of magnitude) [18]. The polarization resistance is inversely proportional to the current density. The polarization resistance increased from 3.16642 to 4.258 MΩ/cm^2. The polarization resistance (R_P) values of 304 SS in 0.5 M NaCl increased from 2.28 MΩ that of the blank to 4.26 MΩ with the immersion period of 24 h. After an immersion of 24 h, the corrosion potential of Al_2O_3 substrate decreased to -306 mV and R_p increased to 4.258×10^6 Ω, respectively, as shown Table 3. The increase in the R_P value suggests that the inhibition efficiency increased with the increase in the immersion time. However, the E_{corr} and R_p value of the alumina coating showed no significant reduction with increasing immersion time. The corrosion potential of uncoated 304 SS was –325 mV and alumina-coated 304 SS samples have E_{corr} ranging from –209 to –306 mV at varying immersion

Table 2: Electrochemical corrosion properties for uncoated 304 SS and alumina coated 304 SS in 0.5M NaCl solution derived from the polarization curves given in Figure 3.

Parameters	Specimen				
	Uncoated 304 SS (0.5 M NaCl)	Alumina coated 304 SS (0.5 M NaCl)			
Sample immersion time	**0 h *(a)***	**0 h *(b)***	**1 h *(c)***	**5 h *(d)***	**24 h *(e)***
E_{corr} (mv)	−325.812	−209.35	−284.54	−288.708	−306.562
I_{corr} (μA/cm^2)	2.008	1.699	1.143	1.172	1.112
Cathodic Tafel slope $\beta_{ca} \times 10^2$ mV /decade	120.307	151.124	111.577	114.516	117.765
Anodic Tafel slope $\beta_{an} \times 10^2$ mV /decade	865.533	682.708	748.160	1218.446	1448.816
Corrosion Rate (MPY)	0.82174	0.69528	0.46775	0.47962	0.4550
Polarization resistance Rp $\times 10^6 \Omega$/cm^2	2.28705	3.16642	3.6934	3.8832	4.2583
Inhibition Efficiency (%)	–	15.38	43.07	41.633	44.62

Table 3: Electrochemical corrosion properties for uncoated 304 SS and alumina coated 304 SS in 1 M NaCl solution derived from the polarization curves given in Figure 4.

Parameters	Specimen				
	Uncoated 304 SS (1 M NaCl)	Alumina coated 304 SS (1 M NaCl)			
Sample immersion time	**0 h *(a)***	**0 h *(b)***	**1 h *(c)***	**5 h *(d)***	**24 h *(e)***
E_{corr} (mv)	−215.695	−307.78	−328.02	−336.14	−356.22
I_{corr} (μA/cm^2)	3.302	2.8253	1.7731	0.9807	3.005
Cathodic Tafel slope $\beta_{ca} \times 10^2$ mV /decade	204.817	141.190	113.784	108.718	131.388
Anodic Tafel slope $\beta_{an} \times 10^2$ mV /decade	1859.342	147.592	175.696	164.112	183.997
Corrosion Rate (MPY)	1.35147	1.1562	0.7256	0.40135	1.2297
Polarization resistance Rp $\times 10^6 \Omega$/cm^2	2.4292	1.11046	1.6934	2.8992	1.1090
Inhibition Efficiency (%)	–	14.43	46.29	70.29	8.99

times such as 0 h, 1 h, 5 h and 24 h. The corrosion current density values of alumina-coated 304 SS have lower values such as 1.699 μA/cm^2, 1.143 μA/cm^2 and 1.1123 μA/cm^2, but after 5 h immersion alumina-coated 304 SS has slightly higher value compared to others. The corrosion current density value decreased from 2.008 μA/cm^2 of the blank to 1.143 μA/cm^2 for an immersion period of 1 h and it is further reduced gradually with increasing immersion time. The corrosion rate of alumina coated 304 SS has higher upon immersion in 1 M NaCl solution compared to immersion in 0.5 M NaCl solution due to different molar concentrations of the solution. However, at alumina-coated 304 SS slower corrosion takes place like 0.4550 and 1.1090 MPY for 24 h immersion in both types of solutions.

Impedance spectra of alumina-coated 304 SS for the different immersion times are illustrated and compared to uncoated 304 SS in Figure 3 and 4. Fitting of spectra was done by an equivalent circuit as shown in Figure 3. The impedance response indicates that the corrosion processes are controlled by mass transport of either reactants (such as dissolved oxygen) or alternatively the formation of corrosion products. Both the 1 h and 5 h plots are characteristic of semi-infinite diffusion indicative of the coating microstructure allowing the oxygen concentration to gradually decrease across the test solution/coating interface. The 24 h plot exhibits a slightly different behavior (*i.e.*, a flat tail) more representative of finite-length diffusion (as shown in Figure 5 (b)) and suggests that there is less open porosity making the diffusion process slow and difficult. These porosity results show that the accumulation of corrosion products in the pore network, which will have the effect of blocking the difficult channels [19]. Figure 5 (a) shows that the impedance plots for the alumina coated 304 SS in 1 M NaCl solution at different immersion times are slightly different to those observed for the immersion of 0.5 M NaCl solutions and are composed of two depressed semicircles. Figure 5 (c) and (d) show that the phase angle decreases drastically at low frequencies. The phase angle starts at 80° for 1 M NaCl and 76° for 0.5 M NaCl solution. In both experiments at increasing immer-

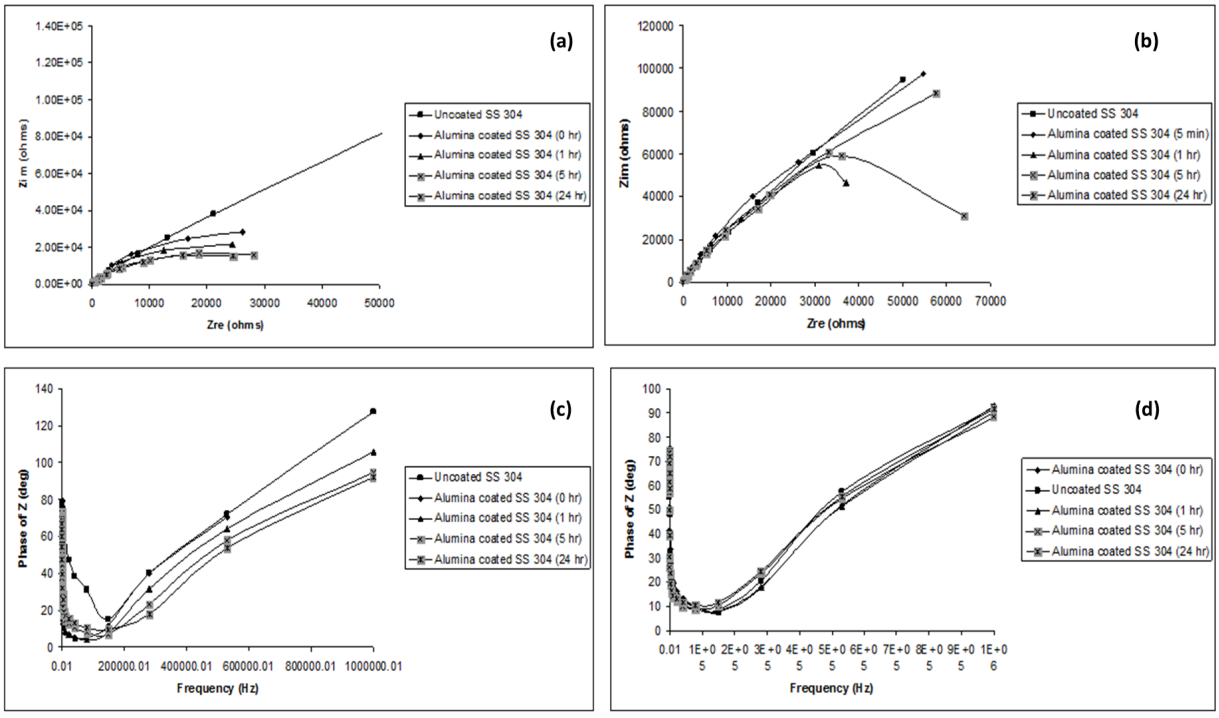

Figure 5: Nyquist plot for alumina coated 304 SS film in (a) 1 M NaCl solution (b) 0.5 M NaCl and Bode phase angle plot of alumina coated 304 SS in (c) 1 M NaCl solution (d) 0.5 M NaCl solution.

sion time the phase angle decreased corresponding to the higher frequency range of 1 MHz, but phase angle slightly varies in 0.5 M NaCl in the range of 85-95° due to the concentration of the solution, which means that the coating porosity increases during exposure to the corrosive solution.

Figure 1(b) and (c) shows XRD-pattern of alumina-coated SS 304 with an immersion period of 24 h in 0.5 M NaCl. This pattern shows the characteristic peak (111) at $2\theta = 18°$, which revealed that formation of Fe_2O_3 into the passive film by the electrochemical corrosion process [JCPDS file No. 39-1346]. The chemical composition of SS 304 has iron as a major component as presented in Table 1. During the electrochemical corrosion Fe was oxidized under atmospheric conditions and converted to Fe_2O_3. Bragg peaks appeared at 2θ position 43°and 74 °demonstrating the presence of α-Al_2O_3. The particle size varies from 10.5 to 13.1 nm.

Alumina-coated SS 304 has same XRD-pattern at different molar concentrations after 24 h immersion. The intensity of Fe_2O_3-peak has varied, an immersion in 1 M NaCl resulted in increased intensity compared to 0.5 M NaCl due to the concentration of the solution as represented in Figure 1 (c). Alumina-coated SS 304 was exposed to the electrochemical corrosion conditions in 1 M and 0.5 M NaCl. Al_2O_3 coated SS in 1M and 0.5 M NaCl is found to have a characteristic peak at $2\theta = 18°$ (Fe_2O_3), 43° and 74°, which can be attributed to the presence of (111), (113) and (208) planes confirming the formation of aluminum oxide and iron oxide. The average particle size is 16 nm. A small amount of Fe_2O_3 may exist in the coatings in the form of a mullite phase, which was formed from the electrolyte constituents (*i.e.*, sodium chloride) during the electrochemical corrosion reaction. Figure 2 (b) shows alumina-coated and uncoated SS 304 after immersion for 24 h in 0.5 M NaCl solution which clearly explains that the alumina-coated surface acts as a corrosion protection. Uncoated SS 304 has darker surface compared to alumina coated surface. Figure 2 (c) refers to the alumina on SS with an inhibition period of 24 h in 1 M NaCl solution. The surface defects were present on the surface due to scrubbing by different grade emery papers used for cleaning the surface. The above images show alumina-coated SS 304 with an exposure period of 24 h in higher molar concentration like 1 M NaCl. Figure 2 (c) indicates that the alumina act as a protective coating material on the SS surface by identifying with the help of uncoated region (right side).

4 Conclusions

The present study deals with the preparation of aluminum oxide on 304 SS from pure aluminum (99.99%) target using DC reactive magnetron sputtering technique. The behavior of alumina-coated 304 SS film in the different concentration of solutions of NaCl was investigated by XRD and SEM analyses. The most suitable sputtering conditions were applied for making well-adhering alumina films on the substrate 304 SS. The effective sputtering current applied to the target was 0.12 A and its corresponding discharge voltage 0.27 kV to avoid target poisoning of the target surface.

XRD pattern demonstrates the crystalline nature of aluminum oxide and its particle dimensions. The alumina-coated 304 SS has the particle size ranging from10.5-13.5 nm. The average size of crystallites in alumina-coated 304 SS film after applying corrosion inhibition in 0.5 M NaCl was estimated to be 16 nm, the values for alumina-coated 304 SS in 1 M NaCl ranged from 10.5 to 13.1 nm. Corrosion protection of alumina-coating on 304 SS was studied at different concentrations of NaCl. The polarization resistance value of alumina coated 304 SS in 0.5 M NaCl increased from 3.1644 to 4.2583 $M\Omega/cm^2$ by increasing the immersion duration. The corrosion potential (E_{corr}) of alumina coated 304 SS in 1 M NaCl increased with the immersion period. The corrosion rate of alumina coated 304 SS was higher in 1 M NaCl solution compared to that in 0.5 M NaCl due to the molar concentration of the solution. However, the corrosion level was quite low (0.4550 and 1.1090 MPY) after 24 h immersion in both solutions. Thus it is known that alumina-coated 304 SS provides chemical inertness, high corrosion resistance and hardness compared to other coating materials like TiC, TiN and TiCN.

Acknowledgement: I thank Dr. R. Saraswathi Professor & Head, Department of Materials Science, School of Chemistry, Madurai Kamaraj University, Madurai, Tamil Nadu, India, for providing necessary facilities and for supervising this work.

References

[1] Ross CA. Properties of radio-frequency-sputtered alumina films on flat and grooved substrates. Journal of Vacuum Science and Technology A., 1996, 14, 2511–2516.

[2] Koski K, Holsa J, Juliet P. Voltage controlled reactive sputtering process for Aluminum oxide thin films. Thin Solid Films, 1998, 326, 189-190.

[3] Sellner S, Gerlach A, Kowarik S, F. Scheiber F, Dosch H, Meyer S, Jens P, Ulbricht G. Comparative study of the growth of sputtered aluminum oxide films on organic and inorganic substrates. Thin solid films, 2008,516, 6377-6381.

[4] Chiang CM, Chang LS. Microstructure and characterization of aluminum oxide thin films prepared by reactive RF magnetron sputtering on copper. Surface Coating and Technology, 2005, 198, 152-155.

[5] Khanna A, Bhat, D.G. Harris A. Beake B.D. Structure-property correlations in aluminum oxide thin films grown by reactive AC magnetron sputtering. Surface and Coating Technology, 2006, 201, 1109-1116.

[6] Hunsicker HY. The Metallurgy of Heat Treatment, Aluminum, Vol. I: Properties, Physical Metallurgy, and Phase Diagrams, American Society for Metals, K. R. Van Horn, 1967.

[7] Edlmayr V, Moser M, Walter C, Mitterer C. Thermal stability of sputtered Al_2O_3 coatings. Surface and Coating Technology, 2010, 204, 1576-1581.

[8] Voigt M, Sokolowski M. Electrical properties of thin rf sputtered aluminum oxide films, Materials Science and Engineering B., 2004,109, 99-103.

[9] Pinto HP, Nieminen RM, Elliot SD. Ab initio study of γ-Al_2O_3 surfaces, Physics Review, 2004, 70, 125402-125413.

[10] Raveh A, Tsameret ZK, Grossman E. Surface characterization of thin layers of Aluminum oxide. Surface and Coating Technology, 1997, 88, 103-111.

[11] Nie X, Meletis EI, Jiang JC, Leyland A, Yerokhin AL, Matthews A. Abrasive wear/corrosion properties and TEM analysis of Al_2O_3coatings fabricated using plasma electrolysis, Surface and Coating Technology, 2002, 149, 245-251.

[12] Cloud AN, Canovic S, Abu-Safe, HH, Gordon MH, Halvarsson M. TEM investigation of alpha alumina films deposited at low temperature. Surface and Coating Technology, 2008, 203, 808-811.

[13] Zywitzki O, Hoetzsch G, Fietzke F, Goedicke K. Effect of substrate temperature on the structure and properties of Al_2O_3 layers reactively deposited by pulsed magnetron sputtering. Surface and Coating Technology, 1996, 82, 169-175.

[14] Yamada – Takamura Y, Koch F, Maier H, Bolt H. Hydrogen permeation barrier performance characterization of vapor deposited amorphous aluminum oxide films using coloration of tungsten oxide. Surface and Coating Technology, 2002, 153, 114-118.

[15] Musil J, Blazek J, Zemen P, Proksova S, Sasek M, Cerstvy R. Thermal stability of alumina thin films containing γ-Al_2O_3 phase prepared by reactive magnetron sputtering. Applied Surface Science, 2010, 257, 1058-1062.

[16] Li N, Allain JP, Ruzic DN. Enhancement of aluminum oxide physical vapor deposition with a secondary plasma. Surface and Coating Technology, 2002, 149, 161-170.

[17] Koski K, Hölsä J, Juliet P. Properties of Aluminum oxide thin films deposited by reactive magnetron sputtering. Thin Solid films, 1999, 139, 240-248.

[18] Li X, Nie X, Wang L, Northwood DO. Corrosion protection properties of anodic oxide coatings on an Al–Si alloy. Surface and Coating Technology, 2005, 200, 1994-2000.

[19] Barik RC, Wharton JA, Wood RJK, Stokes K.R, Jones RL. Corrosion, erosion and erosion–corrosion performance of plasma electrolytic oxidation (PEO) deposited Al_2O_3 coatings, Surface and Coating Technology, 2005, 199, 158-167.